Modelling the Doppler Power Spectrum of Non-Stationary Underwater Acoustic Channels Based on Doppler Measurements

Meisam Naderi [1], Do Viet Ha [2], Van Duc Nguyen [2], and Matthias Pätzold [1]

[1]*Faculty of Engineering and Science, University of Agder, P.O. Box 509, 4879 Grimstad, Norway*
[2]*School of Electronics and Telecommunications, Hanoi University of Science and Technology, Hanoi, Vietnam*
Emails: [1]{meisam.naderi, matthias.paetzold}@uia.no, [2]{dovietha@utc.edu.vn, duc.nguyenvan1@hust.edu.vn}

Abstract—This paper proposes a non-stationary time-continuous simulation model for wideband shallow underwater acoustic (UWA) channels based on measured Doppler power spectrums (DPSs). Measurement-based channel simulators are essential for the test, optimization, and performance analysis of UWA communication systems. The aim is to fit the DPS of the simulation model to that of the measured UWA channel. The performance of the designed UWA channel simulator is assessed by comparing the average Doppler shift and Doppler spread of the channel simulator with the corresponding quantities of the measured UWA channel. The results of the assessment show a good match between the statistical quantities of the UWA channel simulator and those of the real-world UWA channel.

Index terms — Measurement-based channel modelling, shallow underwater acoustic channels, underwater acoustic communications, wideband channels, Doppler power spectrum, Doppler spread.

I. INTRODUCTION

Underwater acoustic (UWA) communication systems have been widely used in various applications in oceanography. For the test, design, and performance analysis of UWA communication systems, the statistical properties of UWA channels in terms of correlation functions, Doppler power spectrum (DPS), and power delay profile (PDP) play an important role. For the performance analysis of UWA communication systems, one usually resorts to computer simulations, which provide a cost-effective and powerful tool to assess the system performance. They can also be used to confirm the correctness of theoretical results obtained analytically.

While many researchers are concerned with the PDPs, the DPS have been less developed for UWA channels [1], [2]. This motivates us to analyze and model the DPS of UWA channels based on Doppler measurements. The Doppler effect in UWA channels is more severe than that in mobile radio channels due to the low speed of sound (1500 m/s), large Doppler frequency shifts with respect to the carrier frequency, and the time-variant characteristics of the surface motion [3]. Therefore, the Doppler effect is indeed a critical issue that affects the performance of UWA communication systems.

In the absence of a standardized model for UWA channels, measurement-based channel modelling is an alternative approach to model the behaviour of real-world UWA channels. However, it is a scenario-specific approach. There are a large number of studies related to the modelling of measurement-based UWA channels. For instance, the distribution of a UWA channel envelope has been reported in [4], [5] to match the Rayleigh distribution, while in [6], [7], it has been shown that the envelope follows the Rice distribution. In addition, the channel envelope may also follow the lognormal distribution as claimed in [8]. These controversial studies show that a realistic UWA channel simulator is necessarily required.

Under the standard assumption of wide-sense stationary uncorrelated scattering (WSSUS), the DPS of UWA channels can be computed by taking the Fourier transform of the autocorrelation function (ACF) of the received signal [9], [10]. However, the WSSUS assumption may not be valid due to the non-stationary behaviour of UWA channels [1].

This paper presents a non-stationary time-continuous simulation model for UWA channels with given DPS obtained from measurements. To obtain the experimental data, we launched a campaign to measure a shallow UWA channel, which was used as a starting point for computing the DPS. The proposed channel simulator has been developed such that its statistical properties (average Doppler shift and Doppler spread) match as close as possible those of the measured real-world channel. For the design of measurement-based channel simulators, we need to determine the model parameters, including the path gains, Doppler frequencies, and phase shifts. Our numerical results show that a good fitting between the measured channel and the simulation model can be achieved with respect to the DPS, average Doppler shifts and Doppler spread.

The rest of this paper is organized as follows. In Section II, the time-continuous channel simulation model is presented. Section III describes the measurement scenario. The numerical results are illustrated in Section IV. Finally, the conclusions are drawn in Section V.

II. NON-STATIONARY TIME-CONTINUOUS CHANNEL SIMULATION MODEL

In this section, we develop a non-stationary time-continuous simulation model for UWA channels using a given DPS. First, the given DPS is presented and then the complex channel gain of the channel simulator is proposed.

A. Given DPS

In the measurement, we assume that the received signal has been stored after each snapshot interval. It is also assumed that the UWA channel is quasi-stationary during each snapshot interval. For the kth snapshot interval of duration T_s, the DPS $\check{S}_{yy}^{(k)}(f,t)$ of the measured UWA channel can be computed as

$$\check{S}_{yy}^{(k)}(f,t) = \sum_{n=1}^{N} \left[c_n^{(k)} \right]^2 \delta(f - f_n^{(k)}) \tag{1}$$

for $t \in [t_k, t_{k+1})$ and $k = 0, 1, 2, \ldots, K-1$. The time interval t_k is defined as $t_k = t_0 + kT_s$ and t_0 equals $T_s/2$. The parameter K denotes the number of snapshots intervals, and thus, the measurement duration T_{mes} is determined by $T_{\text{mes}} = KT_s$. The parameters $c_n^{(k)}$ and $f_n^{(k)}$ denote, respectively, the path gain and Doppler shift of the nth received multipath component for the kth snapshot. The quantity N stands for the number of multipath components in each snapshot. The proof of (1) is provided in the Appendix.

B. Complex Channel Gain

In this paper, we adopt a channel simulation model with complex channel gain $\tilde{\mu}(t)$ based on a sum-of-cisoids uncorrelated scattering (SOCUS) model [11], which is an appropriate channel model for a large class of wideband measured channels under non-isotropic scattering conditions. However, unlike the conventional SOCUS model, the channel gains are time-variant. In the proposed simulation model, for each Doppler shift f_n, we compute time-continuous gains $c_n^{(k)}(t)$ between two consecutive snapshot intervals. The complex channel gain $\tilde{\mu}(t)$ of the non-stationary simulation model can be obtained by $\tilde{\mu}(t) = \sum_{k=0}^{K-1} \tilde{\mu}^{(k)}(t)$, where the kth complex channel gain $\tilde{\mu}^{(k)}(t)$ is given by

$$\tilde{\mu}^{(k)}(t) = \sum_{n=1}^{N'} c_n^{(k)}(t) e^{j(2\pi f_n t + \theta_n)} \tag{2}$$

for $t \in [t_k, t_{k+1})$, where the Doppler frequencies f_n are obtained from the measurement data, and the phase shifts θ_n are unknown and will consequently be modelled as random variables with uniform distribution over $(0, 2\pi]$. The parameter N' denotes the number of cisoids in the simulation model. The time-variant path gain $c_n^{(k)}(t)$ corresponds to the kth snapshot and interpolates the values between two consecutive and constant gains $c_n^{(k)}$ and $c_n^{(k+1)}$, which can be computed by [12, Eq. (6.207)]

$$c_n^{(k)}(t) = \frac{c_n^{(k)} + c_n^{(k+1)}}{2} + \frac{c_n^{(k)} - c_n^{(k+1)}}{2} \cos\left(\frac{\pi(t - t_k)}{T_s} \right) \tag{3}$$

for $t \in [t_k, t_{k+1})$. Note that if $t = t_k$, then $c_n^{(k)}(t) = c_n^{(k)}$ and if $t = t_{k+1}$, then $c_n^{(k)}(t) = c_n^{(k+1)}$.

C. The Spectrogram of the Simulation Model

The spectrogram $\tilde{S}_{yy}(f,t)$ of the simulation model can be obtained by applying the concept of the spectrogram presented in [13]. The spectrogram has been widely used for analyzing

time-variant signals and both stationary and non-stationary processes. In addition, the spectrogram provides variation of the spectral density of a signal (or stochastic process) over time. The spectrogram of a time-varying signal is computed by dividing the signal into overlapping shorter signals and then computing the squared absolute value of the Fourier transform of the short-time signal. However, the spectrogram suffers from a term named cross-term, which is time-variant and depends on the phases. More detailed analysis of the spectrogram can be found in [13]. Let $h(t)$ denote an even and positive window function of the form

$$h(t) = \frac{1}{\sqrt{T}} \text{rect}\left(\frac{t}{T} \right) = \begin{cases} \frac{1}{\sqrt{T}}, & \text{if } -\frac{T}{2} \leq t \leq \frac{T}{2}, \\ 0, & \text{otherwise,} \end{cases} \tag{4}$$

where the parameter T stands for the window length and the function $\text{rect}(\cdot)$ is the rectangular function. The energy of the window function $h(t)$ has been normalized to unity, i.e., $\int_{-\infty}^{\infty} h^2(t)dt = 1$. The short-time Fourier transform (STFT) $\tilde{Y}(f,t)$ of $\tilde{y}(t',t) = \tilde{\mu}(t')h(t' - t)$ is given by (5) (see the bottom of the next page) in which the function $\text{sinc}(\cdot)$ is the sinc function and the symbol $(*)$ denotes the convolutional operator. Note that the window function $h(t')$ is centred at time t. The spectrogram $\tilde{S}_{yy}(f,t)$ of the simulation model is finally obtained as (6) (see the bottom of the next page). The spectrogram $\tilde{S}_{yy}(f,t)$ in (6) reduces to [13, Eq. (11)] if $T \to \infty$ and channel gains are constant, i.e., $c_n^{(k)}(t) = c_n$.

D. Characteristic Quantities

In analogy to [12, Eqs. (7.155) and (7.156)], the time-variant average Doppler shift $\tilde{B}_{yy}^{(1)}(t)$ and the time-variant delay spread $\tilde{B}_{yy}^{(2)}(t)$ of the SOCUS simulation model are defined by the first moment of the spectrogram $\tilde{S}_{yy}(f,t)$ and the square root of the second central moment of the spectrogram $\tilde{S}_{yy}(f,t)$ as

$$\tilde{B}_{yy}^{(1)}(t) = \frac{\int\limits_{-\infty}^{\infty} f\, \tilde{S}_{yy}(f,t)\, df}{\int\limits_{-\infty}^{\infty} \tilde{S}_{yy}(f,t)\, df} \tag{7}$$

and

$$\tilde{B}_{yy}^{(2)}(t) = \sqrt{\frac{\int\limits_{-\infty}^{\infty} f^2\, \tilde{S}_{yy}(f,t)\, df}{\int\limits_{-\infty}^{\infty} \tilde{S}_{yy}(f,t)\, df} - \left(\tilde{B}_{yy}^{(1)}(t) \right)^2} \tag{8}$$

respectively. Analogously, the time-variant average Doppler shift $\check{B}_{yy}^{(1)}(t)$ and the time-variant delay spread $\check{B}_{yy}^{(2)}(t)$ of the measured UWA channel can be computed by

$$\check{B}_{yy}^{(1)}(t) = \frac{\sum_{n=1}^{N} f_n^{(k)} \left[c_n^{(k)} \right]^2}{\sum_{n=1}^{N} \left[c_n^{(k)} \right]^2} \tag{9}$$

and

$$\check{B}_{yy}^{(2)}(t) = \sqrt{\frac{\sum_{n=1}^{N}\left[f_n^{(k)}c_n^{(k)}\right]^2}{\sum_{n=1}^{N}\left[c_n^{(k)}\right]^2} - \left(\check{B}_{yy}^{(1)}(t)\right)^2} \qquad (10)$$

respectively for $t \in [t_k, t_{k+1})$. To study the influence of the parameter N' on the performance of the channel simulator, two error functions $E^{(1)}(N')$ and $E^{(2)}(N')$ are considered as

$$E^{(1)}(N') = \frac{1}{T_{\text{mes}}}\int_0^{T_{\text{mes}}}\left|\tilde{B}_{yy}^{(1)}(t) - \check{B}_{yy}^{(1)}(t)\right|^2 dt \qquad (11)$$

and

$$E^{(2)}(N') = \frac{1}{T_{\text{mes}}}\int_0^{T_{\text{mes}}}\left|\tilde{B}_{yy}^{(2)}(t) - \check{B}_{yy}^{(2)}(t)\right|^2 dt \qquad (12)$$

respectively.

III. MEASUREMENT SCENARIO

To obtain the experimental data, we launched a measurement campaign in West Lake, Hanoi, Vietnam, in June 2016. The measured data was used as a starting point for computing the time-variant DPS $\check{S}_{yy}(f,t)$ of UWA channel. The water depth was about $2.5\,\text{m}$ and the transducer and hydrophone were secured at a depth of $1.5\,\text{m}$. The single-input single-output (SISO) channel measurements were performed at a carrier frequency of $12\,\text{kHz}$ and a signal bandwidth of $4\,\text{kHz}$. The measurement data was collected for two different scenarios. In the first measurement scenario, the initial distance between the receiver and the transmitter was $50\,\text{m}$. Then, the receiver moved away from the fixed transmitter at a speed of about $\text{v}_R = 0.5\,\text{m/s}$ and stopped after travelling $50\,\text{m}$. In the second measurement scenario, the receiver was $100\,\text{m}$ away from the fixed transmitter. Then, the receiver moved towards the transmitter at a speed of about $\text{v}_R = 0.5\,\text{m/s}$ and stopped after passing $50\,\text{m}$.

IV. NUMERICAL RESULTS

In this section, we analyse the statistical properties of the measured UWA channel. Our aim is to develop a non-stationary channel simulation model based on measured DPSs. The performance of the channel simulator has been analyzed by comparing its statistical quantities, including the time-variant average Doppler shift and time-variant Doppler spread, with the corresponding statistical quantities of the measured UWA channel.

The UWA channel has been measured by $K = 20$ snapshots for the first scenario with a snapshot interval of $T_s = 5\,\text{s}$. Hence, the measurement duration T_{mes} of the first scenario was $100\,\text{s}$. In the second scenario, the channel was measured by $K = 24$ snapshots, each one again with the snapshot interval of $T_s = 5\,\text{s}$, i.e., the measurement duration was equal to $T_{\text{mes}} = 120\,\text{s}$.

From the results shown in Figs. 1 and 2, we can conclude that by increasing the number of cisoids N', the error functions in (11) and (12) decrease. As a trade-off between complexity and accuracy, the number of cisoids N' in the simulation setup has been set to 80. The window size T of the spectrogram has been set to $5\,\text{s}$.

Fig. 3 shows the obtained DPS $\check{S}_{\mu\mu}(f,t) = \sum_{k=0}^{K-1}\check{S}_{\mu\mu}^{(k)}(f,t)$ of the first scenario, where negative Doppler frequencies can be observed as expected, because the receiver moves away from the transmitter. As can be seen in this figure, there are strong variations of the gains $c_n^{(k)}$ from one snapshot interval to the next. To address this non-stationary behavior, as stated in Sect. II-B, we propose time-continuous channel gains for the simulation model. Fig. 4 shows the spectrogram $\tilde{S}_{\mu\mu}(f,t)$ of the non-stationary time-continuous simulation model for the first scenario, where a similar trend as for the DPS $\check{S}_{\mu\mu}(f,t)$ of the measured UWA channel can be observed. Similar results have been achieved by comparing the DPS of the measured UWA channel and the spectrogram of the simulation model of the second scenario, which have been presented in Figs. 5 and 4, respectively, where positive Doppler shifts can be observed.

$$\tilde{Y}(f,t) = \int_{-\infty}^{\infty}\tilde{y}(t',t)e^{-j2\pi ft'}dt' = \int_{-\infty}^{\infty}\tilde{\mu}(t')h(t'-t)e^{-j2\pi ft'}dt' = \frac{1}{\sqrt{T}}\int_{-\infty}^{\infty}\sum_{k=0}^{K-1}\sum_{n=1}^{N'}c_n^{(k)}(t')e^{-j[2\pi(f-f_n)t'-\theta_n]}\text{rect}\left(\frac{t'-t}{T}\right)dt'$$

$$= \sqrt{T}\sum_{k=0}^{K-1}\sum_{n=1}^{N'}c_n^{(k)}(f) * \text{sinc}[(f-f_n)T]\,e^{-j[2\pi(f-f_n)t-\theta_n]} \qquad (5)$$

$$\tilde{S}_{yy}(f,t) = \left|\tilde{Y}(f,t)\right|^2 = T\sum_{k=0}^{K-1}\sum_{n=1}^{N'}\left[c_n^{(k)}(f)\right]^2 * \text{sinc}^2[(f-f_n)T]$$

$$+ T\sum_{k=0}^{K-1}\sum_{n=1}^{N'}\sum_{\substack{l=1\\l\neq k}}^{K-1}\sum_{m=1}^{N'}c_n^{(k)}(f)c_m^{(l)}(f) * \text{sinc}[(f-f_n)T]\cdot\text{sinc}[(f-f_m)T]\,e^{-j[2\pi(f_n-f_m)t+\theta_n-\theta_m]} \qquad (6)$$
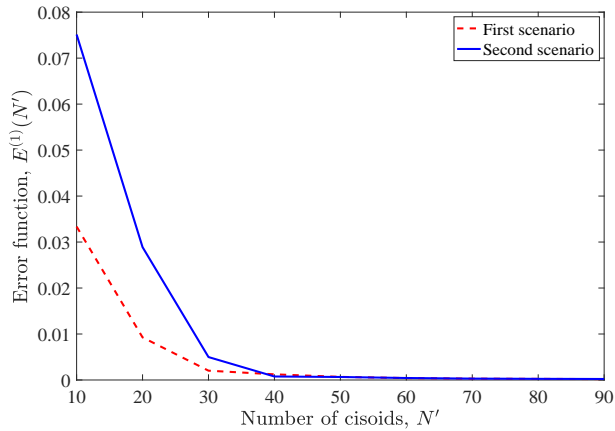
Fig. 1. Evaluation of the error function $E^{(1)}(N')$ in (11) as a function of the number of cisoids N'.
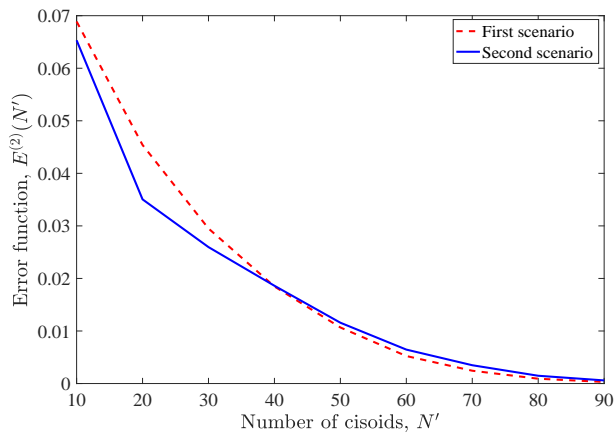

Fig. 2. Evaluation of the error function $E^{(2)}(N')$ in (12) as a function of the number of cisoids N'.
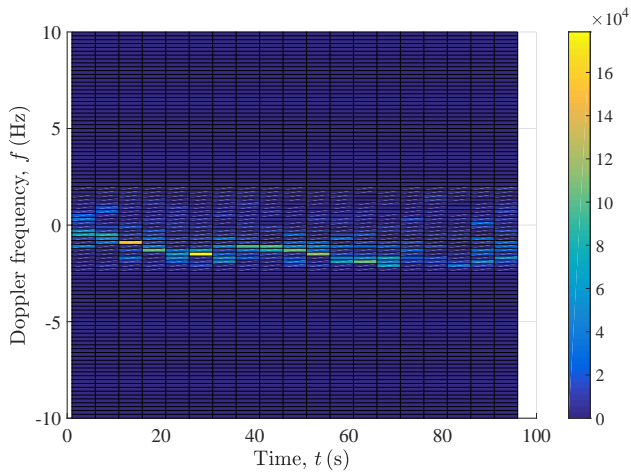

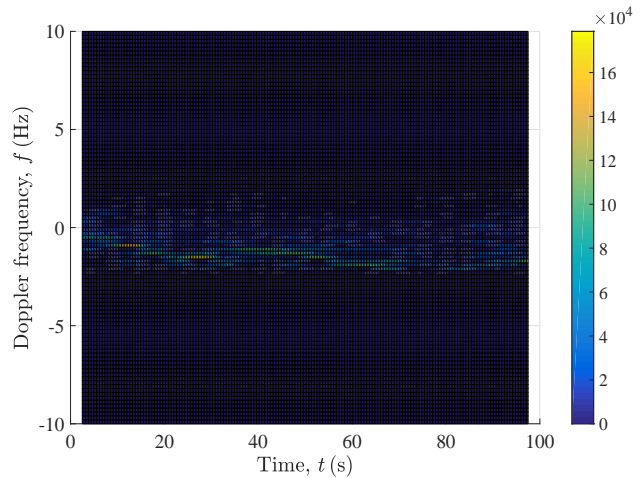Fig. 3. Time-variant DPS $\check{S}_{\mu\mu}(f,t)$ of the measured UWA channel (first scenario).

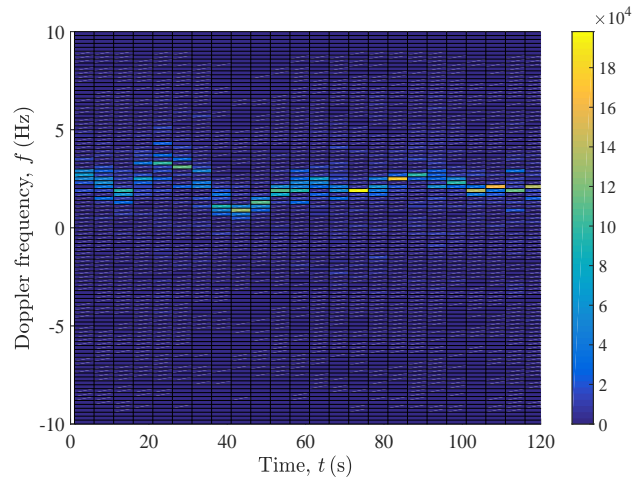Fig. 4. The spectrogram $\tilde{S}_{\mu\mu}(f,t)$ of the simulation model (first scenario).

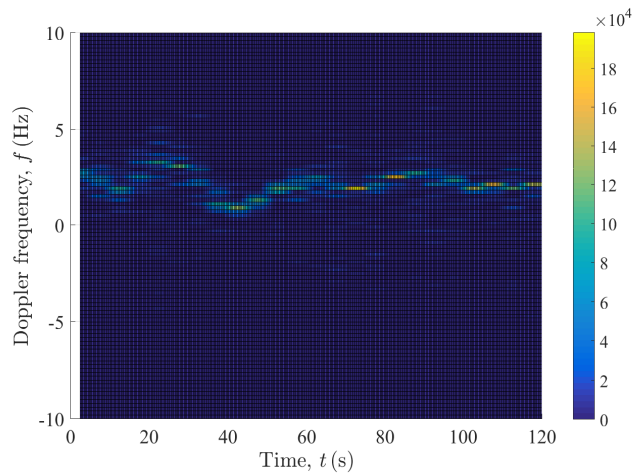Fig. 5. Time-variant DPS $\check{S}_{\mu\mu}(f,t)$ of the measured UWA channel (second scenario).

Fig. 6. The spectrogram $\tilde{S}_{\mu\mu}(f,t)$ of the simulation model (second scenario).
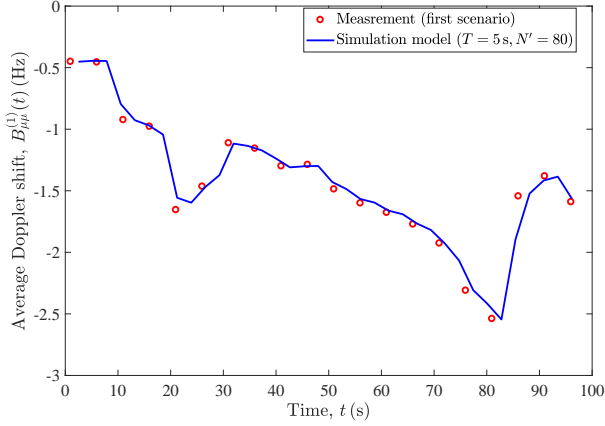
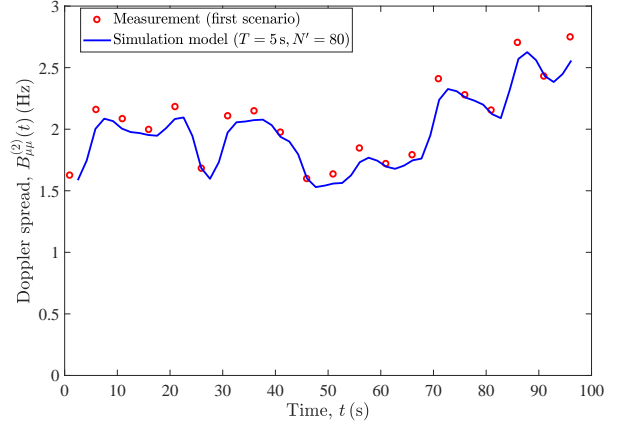Fig. 7.   Time-variant average Doppler shift (first scenario).

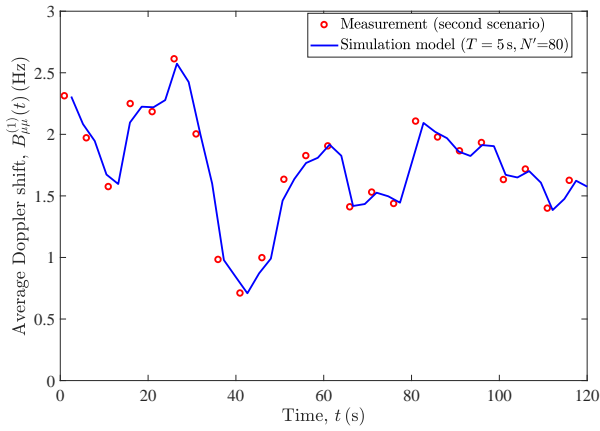Fig. 9.   Time-variant Doppler spread (first scenario).

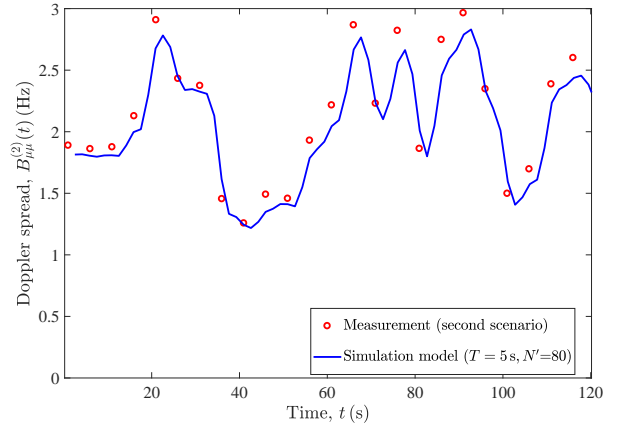Fig. 8.   Time-variant average Doppler shift (second scenario).

Fig. 10.   Time-variant Doppler spread (second scenario).

The results of the assessment show an excellent match between the measured UWA channel and the corresponding simulation model with respect to the time-variant average Doppler shifts $B_{yy}^{(1)}(t)$ obtained for the first scenario and second scenario, as illustrated in Figs. 7 and 8, respectively. As can be seen, unlike stationary channels, the average Doppler shifts change considerably during the measurement duration T_{mes}.

Fig. 9 shows a comparison between the time-variant Doppler spread $\tilde{B}_{yy}^{(2)}(t)$ of the simulation model and that of the measured UWA channel of the first scenario according to (8) and (10), respectively. With reference to this figure, the time-variant Doppler spread of the simulation model follows closely that of the measured UWA channel.

We also analysed the time-variant Doppler spread of the UWA channel for the second scenario as depicted in Fig. 10. As can be seen, a good match has been achieved between the measured UWA channel and the simulation model.

V. CONCLUSION

In this paper, we have presented a non-stationary time-continuous simulation model for UWA channels by means of

measured DPS. We have used an approach to compute time-continuous path gains for the simulation model. The DPS, time-variant average Doppler shift, and time-variant Doppler spread of the channel simulator have been matched to the corresponding quantities of the measured UWA channel. It has been shown that the new channel model provides an excellent fit to measured UWA channels.

APPENDIX

This Appendix presents the proof of (1). The UWA channel is excited by the signal $x(t)$ described by an amplitude A, a carrier frequency f_c, and a phase θ as

$$x(t) = Ae^{j(2\pi f_c t + \theta)}. \tag{13}$$

We assume that the UWA channel is quasi-stationary during each snapshot, and its time-variant channel impulse response $\check{h}^{(k)}(\tau', t)$ can be presented by

$$\check{h}^{(k)}(\tau', t) = \sum_{n=1}^{N} c_n^{(k)} e^{j(2\pi f_n^{(k)} t + \theta_n)} \delta(\tau' - \tau_n') \tag{14}$$

for $k = 0, 1, \ldots, K - 1$. The parameter τ_n' stands for the propagation delay of the nth received component. The received

signal $y^{(k)}(t)$ of the kth snapshot can be computed as

$$
\begin{aligned}
y^{(k)}(t) &= \int_0^\infty x(t - \tau') \check{h}^{(k)}(\tau', t) d\tau' \\
&= A \int_0^\infty e^{j[2\pi f_c(t-\tau')+\theta]} \\
&\quad \times \sum_{n=1}^N c_n^{(k)} e^{j(2\pi f_n^{(k)} t + \theta_n)} \delta(\tau' - \tau'_n) d\tau' \\
&= A e^{j(2\pi f_c t + \theta)} \sum_{n=1}^N c_n^{(k)} e^{j(2\pi f_n^{(k)} t + \theta_n)} \\
&\quad \times \int_0^\infty e^{-j2\pi f_c \tau'} \delta(\tau' - \tau'_n) d\tau' \\
&= x(t) \cdot \sum_{n=1}^N c_n^{(k)} e^{j(2\pi f_n^{(k)} t + \theta_n)} e^{-j2\pi f_c \tau'_n} . \quad (15)
\end{aligned}
$$

The ACF $\check{r}_{yy}^{(k)}(\tau)$ of $y^{(k)}(t)$ can be computed by

$$
\begin{aligned}
\check{r}_{yy}^{(k)}(\tau) &= <y^{(k)*}(t) y^{(k)}(t+\tau)> \\
&= <x^*(t) x(t+\tau) \cdot \sum_{n=1}^N c_n^{(k)} e^{-j(2\pi f_n^{(k)} t + \theta_n)} e^{+j2\pi f_c \tau'_n} \\
&\quad \times \sum_{m=1}^M c_m^{(k)} e^{j[2\pi f_m^{(k)}(t+\tau)+\theta_m]} e^{-j2\pi f_c \tau'_m} >
\end{aligned}
$$
$$(16)$$

where the operator $<\cdot>$ denotes the time average operator. If $n \neq m$, then the ACF $\check{r}_{yy}^{(k)}(\tau) = 0$, and if $n = m$, then the ACF $\check{r}_{yy}^{(k)}(\tau)$ can be obtained as

$$
\begin{aligned}
\check{r}_{yy}^{(k)}(\tau) &= |A|^2 e^{j2\pi f_c \tau} \sum_{n=1}^N \left[c_n^{(k)}\right]^2 e^{j2\pi f_n^{(k)} \tau} \\
&= |A|^2 \sum_{n=1}^N \left[c_n^{(k)}\right]^2 e^{j2\pi(f_c + f_n^{(k)})\tau} . \quad (17)
\end{aligned}
$$

The DPS $\check{S}_{yy}^{(k)}(f)$ of the measured channel of the kth snapshot can be obtained by taking the Fourier transform of the ACF $\check{r}_{yy}^{(k)}(\tau)$ with respect to τ which results in

$$
\check{S}_{yy}^{(k)}(f) = |A|^2 \sum_{n=1}^N \left[c_n^{(k)}\right]^2 \delta(f - f_c - f_n^{(k)}) . \quad (18)
$$

Finally, the time-variant DPS of the measured UWA channel after normalizing with respect to the amplitude squared $|A|^2$ and the carrier frequency f_c can be presented by

$$
\check{S}_{yy}^{(k)}(f, t) = \sum_{n=1}^N \left[c_n^{(k)}\right]^2 \delta(f - f_n^{(k)}) \quad (19)
$$

for $t \in [t_k, t_{k+1})$.

REFERENCES

[1] P. A. van Walree, T. Jenserud, and M. Smedsrud, "A discrete-time channel simulator driven by measured scattering functions," *IEEE J. Sel. Areas Commun.*, vol. 26, no. 9, pp. 1628–1637, Dec. 2008.
[2] S. Watts, L. Rosenberg, S. Bocquet, and M. Ritchie, "Doppler spectra of medium grazing angle sea clutter; part 1: characterisation," *IET Radar, Sonar Navigation*, vol. 10, no. 1, pp. 24–31, 2016.
[3] M. Stojanovic, "Underwater acoustic communications: Design considerations on the physical layer," in *Proc. 5th Annu. Conf. Wireless Demand Netw. Syst. Services (WONS)*, Jan. 2008, pp. 1–10.
[4] M. Naderi, M. Pätzold, and A. G. Zajić, "The design of measurement-based underwater acoustic channel simulators using the INLSA algorithm," in *Proc. IEEE OCEANS*, Genova, Italy, May 2015, pp. 1–6.
[5] F.-X. Socheleau, J. M. Passerieux, and C. Laot, "Characterisation of time-varying underwater acoustic communication channel with application to channel capacity," in *Proc. Underwater Acoust. Meas. Conf.*, Nafplion, Greece, June 2009.
[6] P. Qarabaqi and M. Stojanovic, "Statistical modeling of a shallow water acoustic communication channel," in *Proc. Underwater Acoust. Meas. Conf.*, Nafplion, Greece, Jun. 2009, pp. 1341–1350.
[7] A. Radosevic, J. G. Proakis, and M. Stojanovic, "Statistical characterization and capacity of shallow water acoustic channels," in *Proc. IEEE EUROPE OCEANS*, Bremen, Germany, May 2009, pp. 1–8.
[8] B. Tomasi, P. Casari, L. Badia, and M. Zorzi, "A study of incremental redundancy hybrid ARQ over Markov channel models derived from experimental data," in *Proc. 5th ACM Int. Workshop on UnderWater Networks (WUWNet)*, Massachusetts, USA, Sep./Oct. 2010, pp. 1–8.
[9] C. C. Tsimenidis, B. S. Sharif, O. R. Hinton, and A. E. Adams, "Analysis and modelling of experimental doubly-spread shallow-water acoustic channels," in *Proc. Europe Oceans*, Jun. 2005, vol. 2, pp. 854–858.
[10] H. Lasota and I. Kochańska, "Transmission parameters of underwater communication channels," *Hydroacoustics*, vol. 14, pp. 119–126, 2011.
[11] M. Pätzold and B. Talha, "On the statistical properties of sum-of-cisoids-based mobile radio channel models," in *Proc. 10th Int. Symp. Wireless Pers. Multimedia Commun. (WPMC)*, Jaipur, India, Dec. 2007, pp. 394–400.
[12] M. Pätzold, *Mobile Fading Channels*, Chichester, U.K.: John Wiley & Sons, 2nd edition, 2011.
[13] M. Pätzold and N. Youssef, "Spectrogram analysis of multipath fading channels," in *Proc. 26th IEEE Personal, Indoor and Mobile Radio Communications (PIMRC)*, Hong Kong, China, Aug./Sept. 2015, pp. 2214–2219.